Post-β'' phases and their influence on microstructure and hardness in 6xxx Al-Mg-Si alloys

C. D. MARIOARA*
Department of Synthesis and Properties, SINTEF Materials and Chemistry, 7465 Trondheim, Norway

H. NORDMARK
Department of Physics, Norwegian University of Science and Technology, 7491 Trondheim, Norway

S. J. ANDERSEN
Department of Synthesis and Properties, SINTEF Materials and Chemistry, 7465 Trondheim, Norway

R. HOLMESTAD
Department of Physics, Norwegian University of Science and Technology, 7491 Trondheim, Norway

Published online: 12 January 2006

Starting from solid solution (T4) or a condition with β'' precipitates (T6), three Al-Mg-Si alloys with similar total solute content (1.3 at%), but different Si/Mg ratios (2, 1.25 and 0.8) were isothermally heat-treated at 250 or 260°C and investigated by transmission electron microscopy. The result microstructure for all alloys and conditions consisted of metastable, needle-shaped precipitates growing along ⟨100⟩ directions in aluminium. Each of the phases β''-Mg_5Si_6, β'-$Mg_{1.8}Si$, U1-$MgAl_2Si_2$ and U2-MgAlSi could be identified as main precipitate in the alloy with its solute Si/Mg ratio closest to the same ratio in the composition of that particular phase: The highest Si content alloy produced coarse needles of the trigonal U1-phase coexisting with finer precipitates of hexagonal B′-phase. The most common phase in the Mg-rich alloy is coarse needles of hexagonal β'-type. The Si/Mg ratio of 1.25 in one alloy is similar to the Si/Mg ratio in β''. Here the microstructure changes from that of fine β'' needles to fine needles of the orthorhombic U2-phase. This material remains strongest during heat-treatment. Nucleation on dislocations, mainly by the B′-phase, was observed to be significant in the case of Si-rich alloys heat-treated from T4-condition.

1. Introduction

The Al-Mg-Si alloys constitute a very important industrial group of materials, which is mainly due to their strong age-hardening response. The increase in strength is the result of nucleation and growth in the aluminium matrix of different types of metastable phases. The hardening process is very complex and difficult to optimise, because it is governed by many parameters. In addition to alloy composition, ageing temperature and time, temperature and cooling-rate from solution are important. The storage time at room temperature prior to ageing and how quickly the material is brought to the ageing temperature, affect the nucleation of the precipitates, and may significantly change precipitate number density. In the further development of these alloys quantitative data about the microstructure will be of increasing importance. Information about precipitate types such as composition, their sizes, number density in a condition, is already starting to become important in computer modelling.

*Author to whom all correspondence should be addressed.
0022-2461
DOI: 10.1007/s10853-005-2470-1

In this work alloy composition and starting condition before the ageing heat-treatment are the important variables. Three pure alloys were selected: One alloy was given a Si/Mg-ratio (1.25) close to β''-Mg_5Si_6. While the total amount of solute was kept constant, the other two alloys had a higher content of Mg (Si/Mg = 0.8), and Si (Si/Mg = 2). An earlier study of the same alloys [1] showed that by using a lower, more conventional ageing temperature (175°C), the most Si-rich alloy is the weakest, and the alloys with Si/Mg ratios 1.25 and 0.8 achieved similar strengths. At this temperature GP-zones and β'' are the main precipitates in the peak hardness condition. In order to study the phases that form after β'', the so-called *post*-β'' phases, a higher temperature of the ageing heat-treatment is necessary. At 250°C and 260°C the β''-phase will quickly start to transform/dissolve and one or more of the following types of precipitates will replace it: β', U1, U2 and B′. The phases U1, U2, and B′, are also known as types A, B, and C, respectively [2, 3]. The evolution of metastable phases in the Al-Mg-Si system may be summarised in the following sequence:

SSSS → atomic clusters [4] → GP zones [5, 6] → β'' [6, 7] → β'/B′/U1/U2 [2, 3, 8–11] → β (stable).

Here SSSS is the super-saturated solid solution obtained upon rapid cooling from the solution heat-treatment to room temperature (RT). During the last years, careful analyses of the precipitates have been performed, and crystal structures of all, with the exception of B′-phase have been determined (see Table I). This will aid in the optimisation of alloycomposition to produce a specific type of precipitate so that its influence on material properties may be studied.

2. Experimental

The compositions of the investigated alloys are given in Table II. The total amount of solute was kept constant at 1.3 at%. This is a normal content in important industrial alloys. Alloy A2 is the most Si-rich, A3 has a close Si/Mg ratio to β''-Mg_5Si_6, and A12 is Mg-rich. Each alloy batch weighed 4 kg. The alloys were homogenised 2 h at 570°C and extruded into the shape 2 mm thick bars having a rectangular cross-section (25×2 mm^2). The bars were further cut into lengths of 25 mm.

TABLE II Composition of the investigated alloys

Alloy composition\ designation	Solute content wt%	Solute content at%	Total (Si + Mg) at%	Solute ratio (Si/Mg)
A2	0.88 Si 0.36 Mg	0.8456 Si 0.4 Mg	1.24	2.115
A3	0.75 Si 0.52 Mg	0.721 Si 0.577 Mg	1.3	1.25
A12	0.59 Si 0.65 Mg	0.569 Si 0.723 Mg	1.29	0.8

Heat-treatment H1 consisted of a solution heat-treatment 2 h at 570°C, water-quench to room temperature (RT) and four hours RT-storage before ageing. Prior to ageing the material is in a state similar to the standard T4 condition, and will be denoted so. The H1 samples were quickly heated to 250°C and aged in steps from 10 min to 8 h. After ageing samples were cooled in water.

Heat-treatment H2 consisted of solution heat-treatment 1 h at 540°C, water-quench to RT and four hours storage at RT. The first ageing treatment was 17 h at 175°C. This will be called a T6 condition, although the ageing time is longer than for a typical industrially heat-treated material. The microstructure consists of a high density of fine needles of β''. T6 was the starting point for the final heat-treatment, a quick heating to 260°C followed by ageing 10 min to 5 h. Alloy A2 was not investigated in H2. Lower time and temperature of the solution treatment in H2 were used in order to limit grain-growth. Large grains complicate the TEM investigation since it causes fewer grains to be available for rotating into a ⟨100⟩ Al zone axis. All precipitates in this study are needles aligned parallel to Al ⟨100⟩; the TEM specimens must therefore be tilted to a ⟨100⟩ Al zone axis where quantitative measurements of cross-section and length can be performed, and discrimination between the precipitate types is possible. According to the phase diagram the material is well above solvus line at 540°C. Therefore, the difference in solution temperatures of H1 and H2 should not influence the subsequent precipitation of the two heat treatments. The slightly higher ageing temperature for H2 (260°C) was used in order to avoid excessive salt solidification in the

TABLE I Overview of known precipitation phases in Al-Mg-Si. U1, U2, B′, are also called A, B, C [2, 3]

Phase	Shape	Comp.*	Space group	Lattice parameters (nm)
GP-zones	Needle	Mg_4AlSi_6	C2/m	a = 1.48, b = 0.405, c = 0.648, β= 105.3° [5, 6]
β''	Needle	Mg_5Si_6	C2/m	a = 1.516, b = 0.405, c = 0.674, β= 105.3° [6, 7]
β'	Needle	$Mg_{1.8}Si$	$P6_3$	a = b = 0.715, c = 0.405, γ= 120° [8, 9, 11]
U1	Needle	$MgAl_2Si_2$	$P\bar{3}ml$	a = b = 0.405, c = 0.674, γ= 120° [3, 11]
U2	Needle	MgAlSi	*P*nma	a = 0.675, b = 0.405, c = 0.794 [3, 9]
B′*	Lath	$Mg_9Al_3Si_7$*	Probably $P\bar{6}$	a = b = 1.04, c = 0.405, γ= 120° [10, 11]
β	Plate	Mg_2Si	$Fm\bar{3}m$	a = 0.6354 [9, 11]

*Recent calculations [11] indicate these compositions are energetic favourable. Structure of B′ has not yet been verified with diffraction experiments. It was assumed to be isostructural with the Q-AlMgSiCu phase.

TABLE III Precipitate statistics of the selected specimens

Specimen	Particles/μm^3	Average needle length (nm)	Average cross-section (nm^2)	Volume fraction (%)
H1/A3/10 min	4241 ± 249	116 ± 4	15.3 ± 0.9	0.75
H1/A3/3 h	348.5 ± 31	420 ± 9	65 ± 3.3	0.95
H1/A12/10 min	2651 ± 201	144 ± 3.6	32.55 ± 1.95	1.245
H1/A12/3 h	176.5 ± 8	308 ± 7.4	246 ± 17.6	1.34
H2/A3/10 min	5227 ± 191	100 ± 3.5	17.4 ± 0.9	0.9
H2/A3/3 h	272.5 ± 13	576 ± 19	89 ± 14	1.39
H2/A12/10 min	2271 ± 75	128 ± 4	42.9 ± 3.3	1.245
H2/A12/3 h	139.3 ± 8	426 ± 9.5	258 ± 16.5	1.53

The Si-rich alloy A3 obtains a higher number density of smaller particles as compared to the Mg-rich alloy A12, but lower volume fractions. For similar ageing times a given alloy will end up in very similar microstructures whether the starting condition is T4 (H1) or T6 (H2).

TABLE IV Distribution of phases between the selected conditions, scaled to 100%

Specimen	β'' (%)	β' (%)	U1 (%)	U2 (%)	B′ (%)	Total analysed particles
H1/A3/10 min	76	5	–	19	–	37
H1/A3/3 h	–	26	4.5	65	4.5	23
H1/A12/10 min	8	72	–	17	3	36
H1/A12/3 h	–	96	4	–	–	23
H2/A3/10 min	75	–	15	10	–	30
H2/A3/3 h	–	6	16	72	6	34
H2/A12/10 min	–	100	–	–	–	16
H2/A12/3 h	–	97	–	3	–	18
H1/A2/3 h	–	–	97	–	3	34

β''-Si_6Mg_5 is most common in alloy A3, for short ageing times. The β'-$Mg_{1.8}Si$ phase is stable in the Mg-rich alloy, A12. The U2-AlMgSi phase preferably forms in A3 after longer ageing times. U1-$MgAl_2Si_2$ is the dominant phase in the Si-rich alloy A2. The amount of B′ precipitates may have been underestimated due to the small particle size.

salt bath. In summary, the heat-treatments were designed such that for H1 the post-β'' precipitates originate from a precipitation free SSSS (T4) condition, while in H2 the starting point is a T6-condition with a well developed β'' microstructure. The samples are labelled as Hx/Ay/zmin or zh, where 'x' refers to the type of heat-treatment (H1 or H2), 'y' refers to the alloy (Table II) and 'z' to final ageing time in minutes (zmin) or hours (zh).

Vickers hardness measurements (1 kg load, 10 indentations per sample) were performed for each sample using a Matsuzawa DVK – 1S unit. For the microstructure analysis different samples have been selected to be investigated by TEM (Tables III and IV).

TEM specimens were prepared by electropolishing using a Tenupol 3 machine. The electrolyte consisted of 1/3 HNO_3 in methanol and the solution was kept at a temperature between −20 and −35°C. It was observed that for the Mg-rich A12 alloy some precipitates are destroyed by oxidation during thinning. New specimens were prepared by cold-stage (liquid nitrogen) ion-milling using a Gatan Dual ion-mill machine, model 600 that solved the problem.

A Philips CM30T, operated at 150 kV, was used for the TEM work. This instrument is equipped with a Gatan Parallel EELS (Electron Energy Loss Spectrometer) that enabled determination of specimen thickness of the central area of a micrograph. TEM pictures at different magnifications were recorded on film for the measuring of particle number density, average needle lengths and average cross sections. The precipitate volume fraction for each investigated condition is the product of the precipitate number density, average needle length and average cross section. It gives some information about the amount of solute consumed by the precipitates: One unit cell of β'' ($Si_{12}Mg_{10}$) equals the volume taken by 24 Al atoms. Alloy A3 (see Table II) is optimised for β''. The amount of solute is 1.3 at%. If precipitates were to consume all the solute the volume fraction would be approximately $(24/22) \times 1.3 = 1.42$. Similarly, if the alloy were optimised for β' a maximum fraction would be ∼1.51, while U1 and U2 would give ∼1.42 and 1.50. The maximum error in the estimation of the mean values of the above parameters is on the order of 5% for the number density and 20% for the needle length and cross-section. This gives an error of approximately 30% in the estimated mean volume fraction [as given in Table III]. A more detailed description of the method can be found elsewhere [12]. It is used in other studies as well [13, 14]. The method is simpler to use when the microstructure consists of fine, homogeneous, uniformly distributed particles where errors below 5% can easily be achieved. However, alloy A2 develops a dual precipitate structure consisting of both very coarse and fine precipitates. It was decided to exclude this material from quantification (Table III).

For the particle identification work *nano-diffraction* was employed: A beam with the diameter of approximately 15 nm was moved over the sample. When it hits a needle cross-section, the resulting diffraction pattern was

immediately recorded on film and the particle type could later be identified. 16 to 37 such patterns of arbitrary hits were recorded for each analysed condition (Table IV). The limitation of this method is that very small cross-sections have a lower chance of producing good diffraction patterns. Therefore, the statistics presented in Table IV is probably skewed to precipitates of higher cross-sections. Small particles may be identified by using the TEM in image mode at high magnifications in thin areas. This is a more difficult, uncertain, and time-consuming technique than the nano-diffraction technique, especially since the number densities of particles concerning the present conditions are low.

3. Results

3.1. Hardness curves

The hardness curves for H1 and H2 heat treatments are presented in Fig. 1a and b. In H1 the alloys A3 and A12 have similar hardness values up to 40 min, where the curves split. For the remaining time A3 is harder than A12. A2 starts out with low values, but from about 1 h the hardness is comparable with A12. In the H2 heat treatment both A3 and A12 start off with high hardness because of their initial T6 microstructure. These values are in good agreement with an earlier work [1]. During the heat-treatment at 260°C the hardness of both alloys decreases; the alloys closely follow each other up to 20 min, after which the curves split. Just as for the H1 heat-treatment, A3 is stronger than A12. The overall hardness of both A3 and A12 in H2 is slightly higher as compared to H1.

All the curves have a negative slope suggesting a non-equilibrium situation, where dissolution of one phase and/or nucleation, growth and coarsening of other phases take place.

3.2. Microstructure development

Characteristic TEM images of the microstructure resulting from the H1 and H2 treatments are shown in Figs 2 and 3, respectively. The main conclusions from the analyses are summarised in Table III. The following observations were made:

- The heat-treatments cause precipitates of both A3 and A12 to coarsen. Example: H2/A3/10 min vs. H2/A3/3 h.
- For similar ageing conditions A3 produces a finer precipitate microstructure than A12, and a lower precipitate volume fraction: Compare H1/A3/3 h with H1/A12/3 h.
- A3 and A12 quickly develop similar microstructures regardless of the starting condition (T4 for H1 and T6 for H2). Example: H1/A12/10 min vs. H2/A12/10 min.
- After 3 h ageing A2 develops a dual microstructure consisting of coarse precipitates with low number density and finer precipitates of a high density (Fig. 2e).
- Nucleation on dislocations is observed after short ageing times in the Si-rich A3 alloy for the H1 heat-treatment only (Fig. 2a). H1/A12/10 min also displays nucleation along dislocation lines, but the density is lower than in H1/A3/10 min (Fig. 2b).
- A dense dislocation network connecting the needles forms after 3 h ageing. This is mainly observed in alloys A2 and A12, having coarse microstructures (Fig. 2d and e).

3.3. Phase identification

The fine precipitates that form along dislocation lines in conditions H1/A3/10 min and H1/A12/10 min were studied in more detail. They have typical elongated rectangular cross-sections. Although mainly investigated in the image mode (Figs 2a and 4i), occasional diffraction patterns, as well as the periodicity and appearance in image mode clearly reveal that the majority are of B′ type. In addition, a lower amount of disordered β'', β' and U-phases were also found nucleated on dislocation lines. H1/A2/3 h is another condition with a high density of B′ needles. Here B′

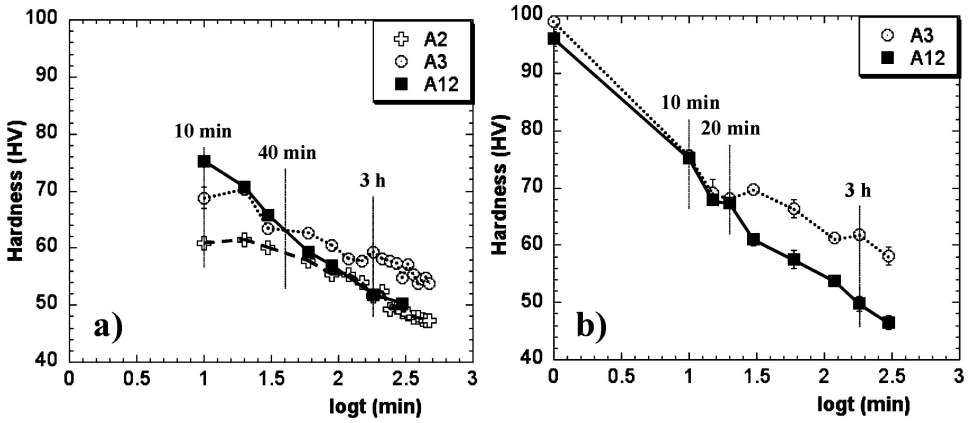

Figure 1 Plots of hardness vs. ageing time of the investigated alloys for heat-treatments H1 (a) and H2 (b). The conditions used for microstructure quantification and phase statistics are found in Tables III and IV, respectively. For both ageing treatments A3 and A12 reach a similar hardness after approximately 15 min, but at longer times A3 is always stronger than A12. A2 in H1 has the lowest hardness.

is confined not only along dislocation lines; larger B′ precipitates are also found inside grains (Fig. 4j). However, the coarsening rate of B′ is always slower than for the other phases identified in these samples; as result its dimensions are usually small. Therefore, it is likely that the number fraction of B′ particles is underestimated for all the investigated conditions in Table IV. The nano-diffraction and high magnification TEM images show that most of the large particles in H1/A2/3 h are U1 (Figs 2e and 4e). Thus, this condition can be characterised as consisting of a low number density of large U1-particles together with a higher density of finer B′ precipitates.

Both H1/A3/10 min (Fig. 2a) and H2/A3/10 min (Fig. 3a) contain dense precipitate microstructures with a significant amount of fine β''-precipitates nucleated homogeneously inside the grains. After three hours annealing U2 becomes the dominant phase in these conditions (Table IV and Fig. 4g). Samples H1/A12/10 min

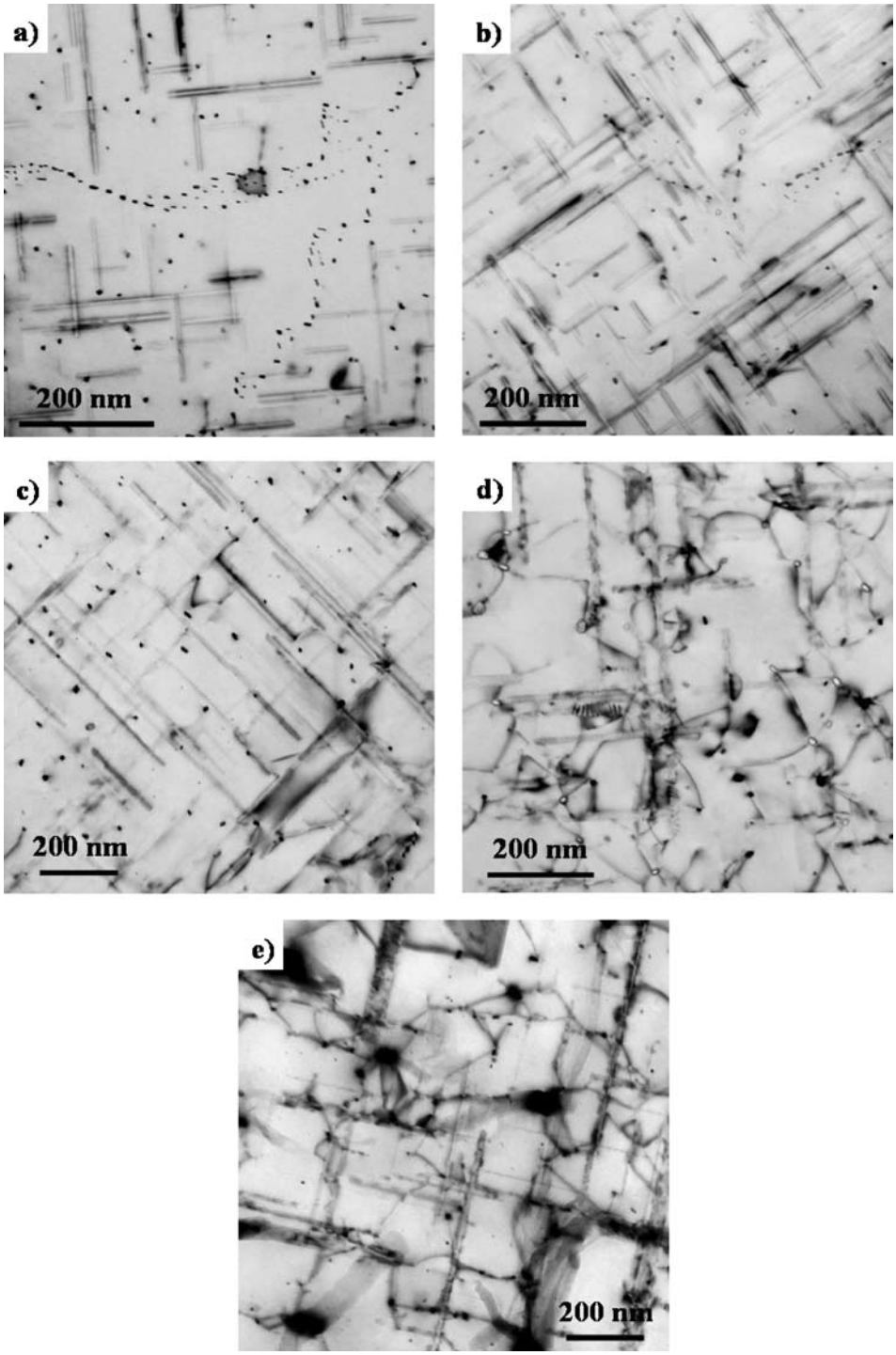

Figure 2 Bright field TEM images from heat-treatment H1: (a) A3/10 min, (b) A12/10 min, (c) A3/3 h, (d) A12/3 h, (e) A2/3 h. In (a), and to a smaller extent in (b) nucleation on dislocations is observed. In (d) and (e) a dense dislocation network appears to connect the needle-shaped precipitates.

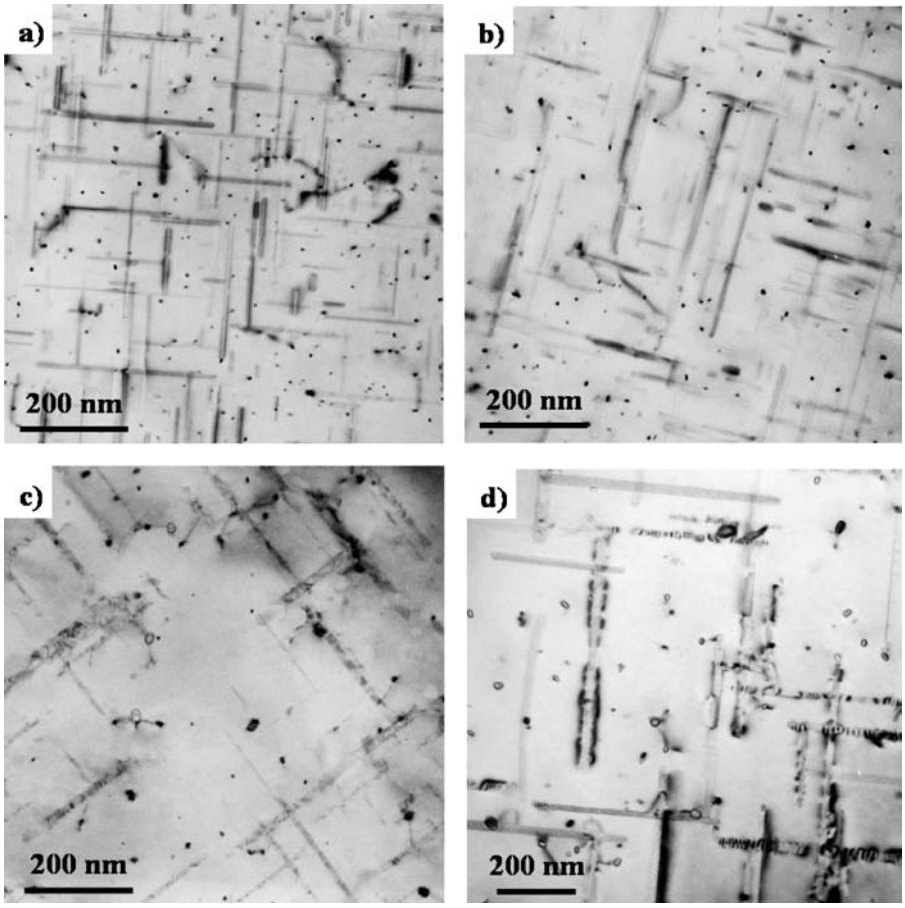

Figure 3 Bright field TEM images from heat-treatment H2: (a) A3/10 min, (b) A12/10 min, (c) A3/3 h, (d) A12/3 h. Microstructures similar to H1 develops, with the exception that nucleation along dislocation lines was not observed.

and H2/A12/10 min follow a different development. Here most of the precipitates are already of β' type after 10 min annealing. β' phase remains stable against transformation and only coarsens during the subsequent ageing (Table IV, Fig. 4c).

3.4. Discussion

An interesting pattern emerges when the occurrence of the different phases is related to the composition of the alloys:

- In alloy A2 (Si/Mg = 2) the main precipitate types are U1-MgA_2lSi_2 and B′.
- Theβ''-Si_6Mg_5 phase survives for longer time in alloy A3 (Si/Mg = 1.25). During the heat treatment β'' dissolves/transforms and U2-MgAlSi becomes the main precipitate.
- In A12 (Si/Mg = 0.8) the β'-$Mg_{1.8}Si$ phase forms after short ageing times and remains stable for the rest of the heat-treatment.

Similar phase occurrence has been found in a recent study by Matsuda [15]. In his work two Cu-free alloys were used, one balanced (Si/Mg = 0.5, Si+Mg = 1.14 wt%), and one excess Si (Si/Mg = 1, Si+Mg = 1.47 wt%). After an annealing heat treatment of 3.3 h at 250°C the typical phase in the balanced alloy was β'. The excess Si alloy produced U2 as dominant phase, while a small amount of U1 was also observed.

An important conclusion is therefore that an alloy tends to select as main phase the precipitate having a Si/Mg ratio closest to the alloy's own Si/Mg ratio. The stability of a precipitate appears to be closely connected to alloy composition. For example, this can explain why the β''-phase survives for 10 min only in alloy A3. The above conclusion applies to both heat-treatments. Fig. 1 together with Tables III and IV show that the occurrence of a precipitate differ only little between H1 and H2, at least after 10 min ageing time. The microstructure transformation from β'' to other phases raises the question whether the dissolution of β'' and the nucleation/growth of phases like β' and U1, U2, are unrelated. The close relationship in atomic structure between these precipitates [9] suggests structural transformation can take place. Another argument for this view is that nucleation along dislocations is observed only in H1. If β'' particles totally dissolve, the same development should also be expected for H2. Since this is not observed, it is more probable that a considerable fraction

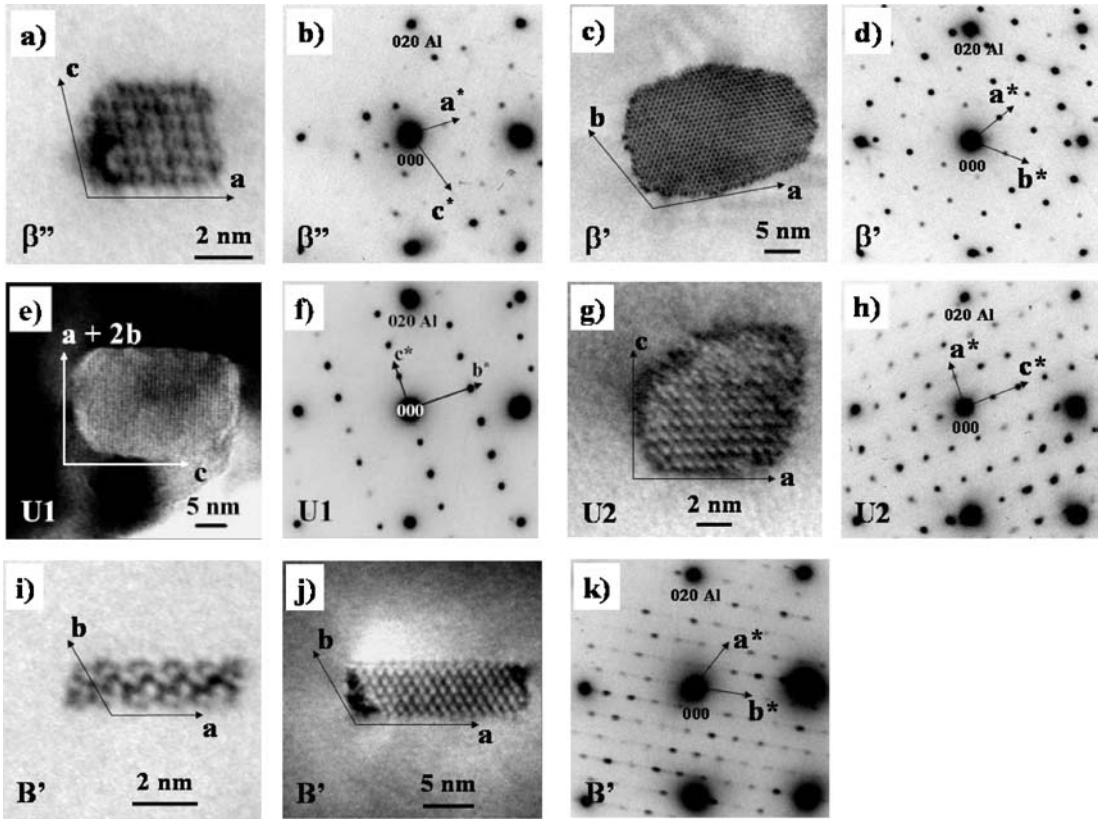

Figure 4 Examples of bright field TEM images and nano-diffraction patterns from various precipitates in the investigated specimens; (a) and (b): β'' in H2/A3/10 min, (c) and (d): β' in H1/A12/3 h, (e) and (f): U1 in H1/A2/3 h, (g) and (h): U2 in H2/A3/3 h. (i): bright field TEM image from a B′ precipitate nucleated on a dislocation in H1/A3/10 min. (j) and (k): B′ precipitate in H1/A2/3 h.

of β'' precipitates nucleates /transforms directly to β', U1, U2. In this way less solute is available in the Al matrix for nucleation of B′. Because in H1 the start microstructure is T4, most solutes are in the matrix and B′ is free to form from the solid solution. In both H1 and H2 heat-treatments A3 produces a finer microstructure with a lower volume fraction as compared to A12. The hardness of these alloys is similar after short ageing times. While the finer particles of A3 are expected to contribute more to hardness, alloy A12 'compensates' with a higher volume fraction (Fig. 1, Table III). A similar situation has been observed at lower temperatures, i.e. 175°C, where most precipitates are of β'' type [1]. However, A3 is always stronger after long ageing times. As noted from Tables III and IV, in both H1 and H2 A12/3 h conditions the cross-sections of β' particles increase much faster than the cross-sections of the U2 precipitates in the A3/3 h samples, while the needle lengths are comparable. This could be related to a more coherent interface between U2 precipitates and the Al matrix, as compared with β' [9]. Since β' loses coherency faster than U2, it also coarsens faster. This would soften the alloy A12 to a limit that cannot be compensated by its higher volume fraction. H1/A2/3 h has a hardness that is comparable to H1/A12/3 h. Although a similar quantification of this condition could not be performed, the coarse U1 microstructure is most probable the cause for the low hardness.

4. Conclusions

- The precipitates developing during ageing at 250 and 260°C in three Al-Mg-Si alloys with a solute content of 1.3 at%, but with different Si/Mg ratios (2, 1.25 and 0.8), were characterised using TEM.
- The condition before ageing was either a supersaturated solid solution (T4) or a microstructure with developed β'' precipitates (T6). After long ageing times, for the same alloy, types and relative amounts of precipitates tend to become similar regardless of the starting condition.
- The phases observed were β''-Mg_5Si_6, β'-$Mg_{1.8}Si$, U1-$MgAl_2Si_2$, U2-MgAlSi and B′.
- The main precipitate-type formed in a given alloy is the one with the Si/Mg ratio most similar to the solute ratio of the alloy.
- After long ageing times the Si-rich alloy A3 is stronger than Mg-rich A12. This corresponds to a higher density of finer U2 precipitates in alloy A3, as compared to the main phase in A12, i.e. β'.
- The main phase in A2 is U1. It coarsens rapidly during the heat-treatment and the hardness decreases to values comparable to A12. Alloy A2 also develops fine precipitates of B′-type.
- Nucleation on dislocations is enhanced in Si-rich alloys and in samples with a T4 initial condition (heat-

treatment H1). Most of the precipitates along dislocation lines are of B′ type.

Acknowledgements

This work was funded through the *NorLight* programme—financed by industry and the *Norwegian Research Council*. Industrial sponsors are the following Norwegian companies: *Hydro Aluminium AS*, *Raufoss ASA* and *Elkem Aluminium*. More information is found at the www address: http://www.sintef.no/norlight/ProjectPortfolio/HeatTreatmentFundamentals/index.htm

References

1. C. D. MARIOARA, S. J. ANDERSEN, H. W. ZANDBERGEN and R. HOLMESTAD, *Met. Mat. Trans. A* (2004) in press.
2. K. MATSUDA, Y. SAKAGUCHI, Y. MIYATA, Y. UETANI, T. SATO, A. KAMIO and S. IKENO, *J. Mater. Sci.* **35** (2000) 179.
3. A. FRØSETH, R. HØIER, P. M. DERLET, S. J. ANDERSEN and C. D. MARIOARA, *Phys. Rev. B.* **67** (2003) 224106.
4. G. A. EDWARDS, K. STILLER, G. L. DUNLOP and M. J. COUPER, *Acta Mater.* **46** (1998) 3893.
5. C. D. MARIOARA, S. J. ANDERSEN, J. JANSEN and H. W. ZANDBERGEN, *ibid.* **49** (2001) 321.
6. P. M. DERLET, S. J. ANDERSEN, C. D. MARIOARA and A. FRØSETH, *J. Phys.: Cond. Matter.* **14** (2002) 4011.
7. S. J. ANDERSEN, H. W. ZANDBERGEN, J. JANSEN, C. TRÆHOLT, U. TUNDAL and O. REISO, *Acta Mater.* **46** (1998) 3283.
8. C. CAYRON and P. A. BUFFAT, *ibid.* **48** (2000) 2639.
9. S. J. ANDERSEN, C. D. MARIOARA, A. FRØSETH, R. VISSERS and H. W. ZANDBERGEN, *Mat. Sci. Eng. A* **390** (2005) 127.
10. S. D. DUMULT, D. E. LAUGHLIN and J. C. WILLIAMS, *Scripta Metallurgica* **18** (1984) 1347.
11. C. RAVI, C. WOLVERTON, *Acta Mater.* **52** (2004) 4213.
12. S. J. ANDERSEN, *Metall. Mater. Trans.* **26A** (1995) 1931.
13. C. D. MARIOARA, S. J. ANDERSEN, J. JANSEN and H. W. ZANDBERGEN, *Acta Mater.* **51** (2003) 789.
14. O. R. MYHR, Ø. GRONG and S. J. ANDERSEN, *ibid.* **49** (2001) 65.
15. K. MATSUDA, S. TANIGUCHI, K. KIDO, Y. UETANI and S. IKENO, *Mater. Trans.* **43** (2002) 2789.

Received 14 December 2004
and accepted 24 May 2005